Supporting Information

Exploring the Origin of Amidase Substrate Promiscuity in CALB by a Computational Approach.

Miquel À. Galmés,[1] Eduardo García-Junceda,[2,*] Katarzyna Świderek,[1,*] Vicent Moliner[1,*]

[1] Departament de Química Física i Analítica, Universitat Jaume I, 12071 Castellón, Spain.

[2] Departamento de Química Orgánica Biológica, Instituto de Química Orgánica General, CSIC Juan de la Cierva 3, 28006 Madrid, Spain.

* corresponding authors:

Eduardo García-Junceda,
e-mail: eduardo.junceda@csic.es

Katarzyna Świderek,
e-mail: swiderek@uji.es

Vicent Moliner,
e-mail: moliner@uji.es

KEYWORDS: Computational chemistry, Enzyme catalysis, Enzyme promiscuity, QM/MM, Molecular Dynamics, Free Energy Surfaces

TABLE OF CONTENTS

COMPUTATIONAL METHODS

Computational details of the molecular models set up

Initial geometry of the protein was obtained from the PDB structure of *Candida antarctica* Lipase B (PDB ID: 1TCA).[1] The protonation state of titratable residues were determined at pH equivalent to 7 using the semiempirical program PropKa ver. 3.0.3.[2,3] The calculations determined that Asp134 must be protonated and all histidines as neutral with hydrogen atom added in Nδ position. Moreover, three disulphide bridges between residues Cys22 and Cys64, Cys216 and Cys258, and Cys293 and Cys311 were identified. Hydrogen atoms were added to the structure and the system was solvated by placing it in a 100 × 80 × 80 $Å^3$ pre-equilibrated box of water molecules. Any water with an oxygen atom lying in a radius of 2.8 Å from a heavy atom of the protein was deleted. The geometry of the system was optimized using a series of optimization algorithms.[4] A final equilibration was done to fully relax the entire system. In order to study the amidase activity of CALB, the system was set up by building the corresponding substrates, benzylbutyramide (**1**) and N-(4-nitrophenyl)-butyramide (**2**), into the active site pocket of a pre-equilibrated CALB.[4] In order to equilibrate the total system a classical MD simulation was done to the Michaelis complex of each system. Substrates were parametrized with Antechamber[5] at AM1 level. Parameters for **1** and **2** are showed in Tables S1 and S2, respectively. Finally 5 ns of classical MD using the NVT ensemble were run to equilibrate the system with AMBER force field,[6] as implemented in NAMD software.[7] In order to avoid the diffusion of the substrate, the distance between OG_{Ser105} and $C1_{Subs}$ was constraint applying a force constant of 2000 $kJ \cdot mol^{-1} \cdot Å^{-2}$.

Table S1. Atom types, charges and parameters obtained for **1**.

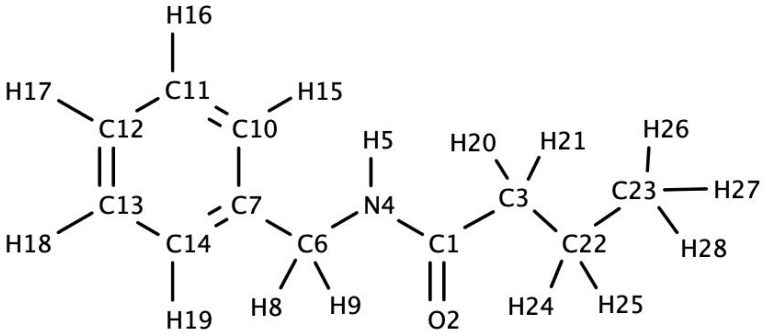

Atom name	Atom type	Charge	Atom name	Atom type	Charge
C23	c3	-0.0941	C6	c3	0.1233
H26	hc	0.0374	H8	h1	0.0712
H27	hc	0.0374	H9	h1	0.0712
H28	hc	0.0374	C7	ca	-0.1213
C22	c3	-0.0784	C10	ca	-0.1175
H24	hc	0.0447	H15	ha	0.1355
H25	hc	0.0447	C11	ca	-0.1315
C3	c3	-0.1564	H16	ha	0.1330
H20	hc	0.0727	C12	ca	-0.1240
H21	hc	0.0727	H17	ha	0.1320
C1	c	0.6511	C13	ca	-0.1315
O2	o	-0.6061	H18	ha	0.1330
N4	n	-0.5569	C14	ca	-0.1175
H5	hn	0.3015	H19	ha	0.1355

Parameters:

MASS

c3	12.01	0.878
hc	1.008	0.135
c	12.01	0.616
o	16.00	0.434
n	14.01	0.530
hn	1.008	0.161
h1	1.008	0.135
ca	12.01	0.360
ha	1.008	0.135

BOND

c3-hc	330.60	1.097
c3-c3	300.90	1.538
c3-c	313.00	1.524
c -o	637.70	1.218
c -n	427.60	1.379
n -hn	403.20	1.013
n -c3	328.70	1.462
c3-h1	330.60	1.097
c3-ca	321.00	1.516
ca-ca	461.10	1.398
ca-ha	345.80	1.086

ANGLE

c3-c3-hc	46.340	109.800
c3-c3-c3	62.860	111.510
hc-c3-hc	39.400	107.580
c3-c3-c	63.270	111.040
c3-c -o	67.400	123.200
c3-c -n	66.790	115.180
hc-c3-c	46.930	108.770
c -n -hn	48.330	117.550
c -n -c3	63.390	120.690
o -c -n	74.220	123.050
n -c3-h1	49.840	108.880
n -c3-ca	66.210	112.380
hn-n -c3	45.800	117.680
c3-ca-ca	63.530	120.770
h1-c3-h1	39.240	108.460
h1-c3-ca	46.990	109.560
ca-ca-ha	48.180	119.880
ca-ca-ca	66.620	120.020

DIHEDRALS

c3-c3-c3-hc	1	0.160	0.000	3.000
c3-c3-c3-c	1	0.156	0.000	3.000
hc-c3-c3-hc	1	0.150	0.000	3.000
c3-c3-c -o	1	0.000	180.000	2.000
c3-c3-c -n	1	0.100	0.000	-4.000
c3-c3-c -n	1	0.070	0.000	2.000
hc-c3-c3-c	1	0.156	0.000	3.000
c3-c -n -hn	1	2.500	180.000	2.000
c3-c -n -c3	1	0.000	0.000	-2.000
c3-c -n -c3	1	1.500	180.000	1.000
hc-c3-c -o	1	0.800	0.000	-1.000
hc-c3-c -o	1	0.000	0.000	-2.000
hc-c3-c -o	1	0.080	180.000	3.000
hc-c3-c -n	1	0.000	180.000	2.000
c -n -c3-h1	1	0.000	0.000	2.000
c -n -c3-ca	1	0.000	0.000	2.000
o -c -n -hn	1	2.500	180.000	-2.000
o -c -n -hn	1	2.000	0.000	1.000
o -c -n -c3	1	2.500	180.000	2.000
n -c3-ca-ca	1	0.000	0.000	2.000
hn-n -c3-h1	1	0.000	0.000	2.000
hn-n -c3-ca	1	0.000	0.000	2.000
c3-ca-ca-ha	1	3.625	180.000	2.000
c3-ca-ca-ca	1	3.625	180.000	2.000
h1-c3-ca-ca	1	0.000	0.000	2.000
ca-ca-ca-ha	1	3.625	180.000	2.000
ca-ca-ca-ca	1	3.625	180.000	2.000
ha-ca-ca-ha	1	3.625	180.000	2.000

IMPROPER

c3-n -c -o	10.5	180.0	2.0	General improper torsional angle (2 general atom types)
c -c3-n -hn	1.1	180.0	2.0	
c3-ca-ca-ca	1.1	180.0	2.0	
ca-ca-ca-ha	1.1	180.0	2.0	General improper torsional angle (2 general atom types)

NONBON

c3	1.9080	0.1094
hc	1.4870	0.0157
c	1.9080	0.0860
o	1.6612	0.2100
n	1.8240	0.1700
hn	0.6000	0.0157
h1	1.3870	0.0157
ca	1.9080	0.0860
ha	1.4590	0.0150

Table S2. Atom types, charges and parameters obtained for **2**.

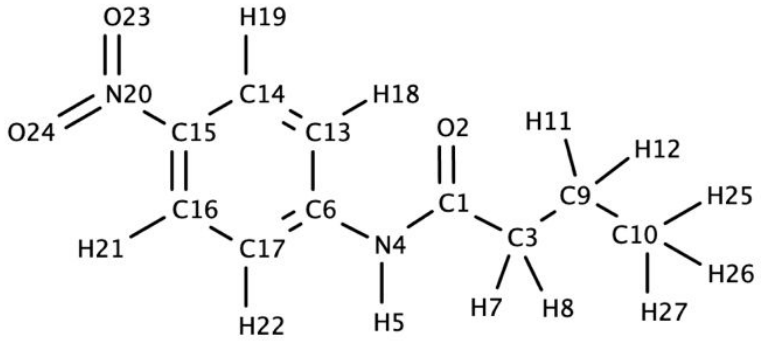

Atom name	Atom type	Charge	Atom name	Atom type	Charge
C10	c3	-0.0981	C6	ca	0.1226
H25	hc	0.0370	C13	ca	-0.1920
H26	hc	0.0370	H18	ha	0.1650
H27	hc	0.0370	C14	ca	-0.0360
C9	c3	-0.0864	H19	ha	0.1715
H11	hc	0.0552	C15	ca	-0.2172
H12	hc	0.0552	N20	no	0.3192
C3	c3	-0.1584	O23	o	-0.2145
H7	hc	0.0812	O24	o	-0.2145
H8	hc	0.0812	C16	ca	-0.0360
C1	c	0.6681	H21	ha	0.1715
O2	o	-0.5731	C17	ca	-0.1920
N4	n	-0.4731	H22	ha	0.1650
H5	hn	0.3235			

Parameters:

MASS

c3	12.01	0.878
hc	1.008	0.135
c	12.01	0.616
o	16.00	0.434
n	14.01	0.530
hn	1.008	0.161
ca	12.01	0.360
ha	1.008	0.135
no	14.01	0.530

BOND

c3-hc	330.60	1.097
c3-c3	300.90	1.538
c3-c	313.00	1.524
c -o	637.70	1.218
c -n	427.60	1.379
n -hn	403.20	1.013
n -ca	384.20	1.412
ca-ca	461.10	1.398
ca-ha	345.80	1.086
ca-no	321.70	1.469
no-o	741.80	1.226

ANGLE

c3-c3-hc	46.340	109.800
c3-c3-c3	62.860	111.510
hc-c3-hc	39.400	107.580
c3-c3-c	63.270	111.040
c3-c -o	67.400	123.200
c3-c -n	66.790	115.180
hc-c3-c	46.930	108.770
c -n -hn	48.330	117.550
c -n -ca	63.820	123.710
o -c -n	74.220	123.050
n -ca-ca	67.870	120.190
hn-n -ca	47.630	116.000
ca-ca-ha	48.180	119.880
ca-ca-ca	66.620	120.020
ca-ca-no	66.770	119.010
ca-no-o	68.700	117.760
o -no-o	76.730	125.080

DIHEDRALS

c3-c3-c3-hc	1	0.160	0.000	3.000
c3-c3-c3-c	1	0.156	0.000	3.000
hc-c3-c3-hc	1	0.150	0.000	3.000
c3-c3-c -o	1	0.000	180.000	2.000
c3-c3-c -n	1	0.100	0.000	-4.000
c3-c3-c -n	1	0.070	0.000	2.000
hc-c3-c3-c	1	0.156	0.000	3.000
c3-c -n -hn	1	2.500	180.000	2.000
c3-c -n -ca	1	2.500	180.000	2.000
hc-c3-c -o	1	0.800	0.000	-1.000
hc-c3-c -o	1	0.000	0.000	-2.000
hc-c3-c -o	1	0.080	180.000	3.000
hc-c3-c -n	1	0.000	180.000	2.000
c -n -ca-ca	1	0.450	180.000	2.000
o -c -n -hn	1	2.500	180.000	-2.000
o -c -n -hn	1	2.000	0.000	1.000
o -c -n -ca	1	2.500	180.000	2.000
n -ca-ca-ha	1	3.625	180.000	2.000
n -ca-ca-ca	1	3.625	180.000	2.000
hn-n -ca-ca	1	0.450	180.000	2.000
ca-ca-ca-ha	1	3.625	180.000	2.000
ca-ca-ca-ca	1	3.625	180.000	2.000
ca-ca-ca-no	1	3.625	180.000	2.000
ha-ca-ca-ha	1	3.625	180.000	2.000
ca-ca-no-o	1	0.600	180.000	2.000
ha-ca-ca-no	1	3.625	180.000	2.000

IMPROPER

c3-n -c -o	10.5	180.0	2.0	General improper torsional angle (2 general atom types)
c -ca-n -hn	1.1	180.0	2.0	General improper torsional angle (2 general atom types)
ca-ca-ca-n	1.1	180.0	2.0	Using default value
ca-ca-ca-ha	1.1	180.0	2.0	General improper torsional angle (2 general atom types)
ca-ca-ca-no	1.1	180.0	2.0	Using default value
ca-o -no-o	1.1	180.0	2.0	Using default value

NONBON

c3	1.9080	0.1094
hc	1.4870	0.0157
c	1.9080	0.0860
o	1.6612	0.2100
n	1.8240	0.1700
hn	0.600	0.0157
ca	1.9080	0.0860
ha	1.4590	0.0150
no	1.8240	0.1700

Computational details of the QM/MM simulations

In this work, an additive hybrid QM/MM scheme was employed for the construction of the total Hamiltonian, $\hat{H}_{eff}$, where the total energy is obtained from the sum of each contribution to the energy.

$$\hat{H}_{eff} = \hat{H}_{QM} + \hat{H}^{elec}_{QM/MM} + \hat{H}^{VdW}_{QM/MM} + \hat{H}_{MM} \quad \text{(S1)}$$

Here, $\hat{H}_{QM}$ describes the atoms in the QM part, $\hat{H}_{QM/MM}$ defines the interaction between the QM and MM region and $\hat{H}_{MM}$ describes the rest of the MM part.

Potential Energy Surfaces

Exploration of the Potential Energy Surfaces (PES) was carried out by choosing the appropriate combination of internal coordinates (ξ_i) in every single step of the reaction. A harmonic constraint was used to maintain the proper interatomic distances along the reaction coordinate, and a series of conjugate gradient optimizations and L-BFGS-B optimization algorithms were applied to obtain the final potential energy of the minimized constrained geometry. The QM sub-set of atoms were described by the Austin Model 1 (AM1)[8] semiempirical Hamiltonian.

After the exploration of stationary points on the PES, the structures corresponding to reactants and products states (RS and PS, respectively), intermediates (Is) and transition state (TSs) were localized applying the Baker's algorithm.[9] Minimum energy path was traced down to reactants and products following the Intrinsic Reaction Coordinate[10] (IRC) method from every localized TS structure.

Spline corrections

A correction term is interpolated to any value along the reaction coordinates in the FES. A continuous energy function is used to obtain the corrected PMFs:

$$E = E_{LL/MM} + S[\Delta E_{LL}^{HL}(\xi_1,\xi_2)] \quad \text{(S2)}$$

where *S* is the two-dimensional spline function and ΔE_{LL}^{HL} is the difference between the energies obtained at low-level (LL) and high-level (HL) of theory of the QM part. The AM1 semiempirical Hamiltonian was used as LL method, while a density functional theory (DFT)-based method was selected for the HL energy calculation. In particular, HL energy calculations were performed by means of the hybrid M06-2X[11] functional using the standard 6-31+G(d,p) basis set. These calculations were carried out using the Gaussian09 program.[12]

Free Energy Surfaces

FESs were obtained, in terms of 2D-PMF,[13] for every step of the reaction using the Umbrella Sampling approach[13,14] combined with the Weighted Histogram Analysis Method (WHAM).[15] Series of MD simulations were performed adding a constraint along the selected reaction coordinates with an umbrella force constant of 2500 kJ·mol^{-1}·Å^{-2}. In every window QM/MM MD simulations were performed with a total of 5 ps of equilibration and 20 ps of production at 303 K using the Langevin-Verlet algorithm[16] with a time step of 1 fs. Structures obtained in previously computed PESs were used as starting points for the MD simulations in every window.

Kinetic Isotope Effects

Averaged KIEs were calculated from isotopic substitution of the key atoms from localized RS and TS structures. From the definition of the free energy of a state and using the Transition State

Theory, the ratio between the rate constants corresponding to the heavy and the light atoms can be computed by means of equation S3.

$$KIE = \frac{\left(\frac{Q_{TS}}{Q_{RS}}\right)_L}{\left(\frac{Q_{TS}}{Q_{RS}}\right)_H} e^{(-1/(RT))(\Delta ZPE_L - \Delta ZPE_H)} \quad \text{(S3)}$$

Here, Q refers to the total partition function which was computed as the product of the translational, rotational and vibrational partition functions of isotopologs in RS and TS structures, and ΔZPE refers to difference of the zero point energy between RS and TS in the light (L) and heavy (H) isotopologs.[17,18] KIEs were computed at M06-2X/MM and AM1/MM level of theory. In the case of AM1/MM KIEs, ten structures representing each of the TS and the RS were extracted from a MD simulation constraining the key distances to maintain their characteristic geometries. These structures were localized to have 10 representative structures of each state. Those were used to compute the averaged KIEs. The Hessian was computed for the QM subset of atoms. For M06-2X/MM KIEs, one RS structure and one TS structure for each step of the reaction were localized at this high level of theory.

EXPERIMENTAL METHODS

Synthesis of benzylbutyramide (1)

The synthesis of the substrate benzylbutyramide was carried out following an enzymatic approach. Commercial immobilized CALB (Novozyme 435) was used to synthetize **1**, from benzylamine and butyric acid. Equimolar solution of 50 mM of butyric acid and benzylamine in 2-methyl-2-butanol, was incubated during 120 hours in sealed vessels with argon atmosphere and molecular sieves to minimize the available soluble water that is formed in the reaction. The reaction was followed by Thin-Layer Chromatography (TLC), with a mobile phase of hexane:ethyl acetate (2:3), until complete conversion. The product was purified by Silica column with hexane:ethyl acetate (1:5) as mobile phase. Solvent was finally evaporated in a rotatory evaporator, obtaining pure product, which was characterized by mass spectrometry (m/z = 178.2) and NMR (Figure S1). The overall yield obtained was of 48%.

Synthesis of N-(4-nitrophenyl)-butyramide (2)

Butyryl chloride dissolved in 5 mL anhydrous dichloromethane (4.32 mmols) was added to 10 mL of a solution of 4-nitroaniline (3.60 mmols) with pyridine (7.20 mmols) in anhydrous dichloromethane to act as a base to catalyze the reaction. The molar ration of butyryl chloride:4-nitroaniline:pyridine was set to 1.2:1:2. Reaction was performed in sealed vessels in argon atmosphere at room temperature over-night. Once reaction was completed, further washes with 10% HCl were performed. **2** was purified by Silica column with hexane:ethyl acetate (4:1) as mobile phase. Solvent was evaporated in a rotatory evaporator obtaining yellow crystals. The product was characterized by NMR (Figure S2) and the overall yield was 74%.

Enzymatic assays of the hydrolysis of 1.

In order to evaluate the amidase reaction of CALB, experimental kinetics parameters of hydrolysis of **1** were obtained. Commercial free form of wild type CALB was purchased from Sigma-Aldrich. Kinetics assays were performed in 20 mM phosphate buffer at pH 7, with 10 % of organic solvent, acetonitrile in this case. The addition of organic solvent is due to the poor solubility of **1** in aqueous solution. Different organic solvents were discarded due to interferences with the signal during HPLC acquisitions. Real concentration of enzyme in the commercial powder was determined by Bradford. Final concentration of enzyme in the assay was adjusted to 105 $\mu g \cdot mL^{-1}$ and concentrations of **1** were set to 0 mM, 0.2 mM, 0.5 mM, 1 mM, 5 mM in a final volume of 500 µL. Reactions were done at 37 ^{o}C and 100 rpm. Aliquots of 50 µL were taken at 0 h, 3 h, 5 h, 7h, 24 h and 48 h, and were frozen at -20 ^{o}C to stop the progression of the reaction.

Formation of the benzylamine was monitored by HPLC (JASCO UK Limited). A diluted sample of each aliquot was injected into a C18 column and a mixture of water:acetonitrile 50:50 with 0.5 % of trifluoroacetic acid was used as a mobile phase with a 1 $mL \cdot min^{-1}$ flow. Elution of products (benzylamine) was followed by absorbance at 206 nm (retention time of benzylamine = 3.1 min; retention time of benzylbutyramide = 4.5 min).

Enzymatic assays of the hydrolysis of 2

To assay the amidase activity on **2** commercial wild type CALB was used (Sigma-Aldrich). The poor solubility of the substrate makes impossible to perform reactions in pure aqueous solutions so addition of organic solvent is required. Reactions were done in 20 mM phosphate buffer at pH 7, with 10 % of DMSO. Concentrations of **2** were set to 0 mM, 0.5 mM, 1.0 mM, 1.5 mM, 2.0 mM, 2.5 mM and 3 mM and final concentration of protein was set to 35 $\mu g \cdot mL^{-1}$. Reactions were

carried out in a final volume of 150 µL in microtiter plates at 37 ºC and 100 rpm. Reactions were done in triplicates. The progression of the reaction was monitored during 24 hours by the increment of absorbance at 405 nm using a spectrophotometer (Spectra max Plus 384 from Molecular Devices). The use of this spectrophotometric technique permits the use of DMSO instead of acetonitrile in the case of **2**. The use of spectrophotometric approaches is not possible in the case of **1**, because of the very high similar peaks of absorbance of substrates and products (maximum absorbance peak of **1**, substrate: 250 nm; and benzylamine, product: 245 nm).

RESULTS

NMR Spectra of the substrates

^{1}H NMR spectra were done to characterize the substrates. Spectra for **1** is depicted in Figure S1 and for **2** in Figure S2.

Benzylbutyramide: ^{1}H NMR (300 MHz, Chloroform-*d*) δ 7.47 – 7.17 (m, 3H), 5.76 – 5.67 (m, 1H), 4.44 (d, *J* = 5.7 Hz, 1H), 2.32 – 2.00 (m, 6H), 1.85 – 1.54 (m, 2H), 1.14 – 0.82 (m, 2H).

N-(4-nitrophenyl)-butyramide: ^{1}H NMR (300 MHz, Chloroform-*d*) δ 8.27 – 8.16 (m, 2H), 7.76 – 7.65 (m, 2H), 7.37 (s, 2H), 2.40 (dd, *J* = 7.8, 7.1 Hz, 2H), 1.88 – 1.69 (m, 2H), 1.03 (t, *J* = 7.4 Hz, 3H).

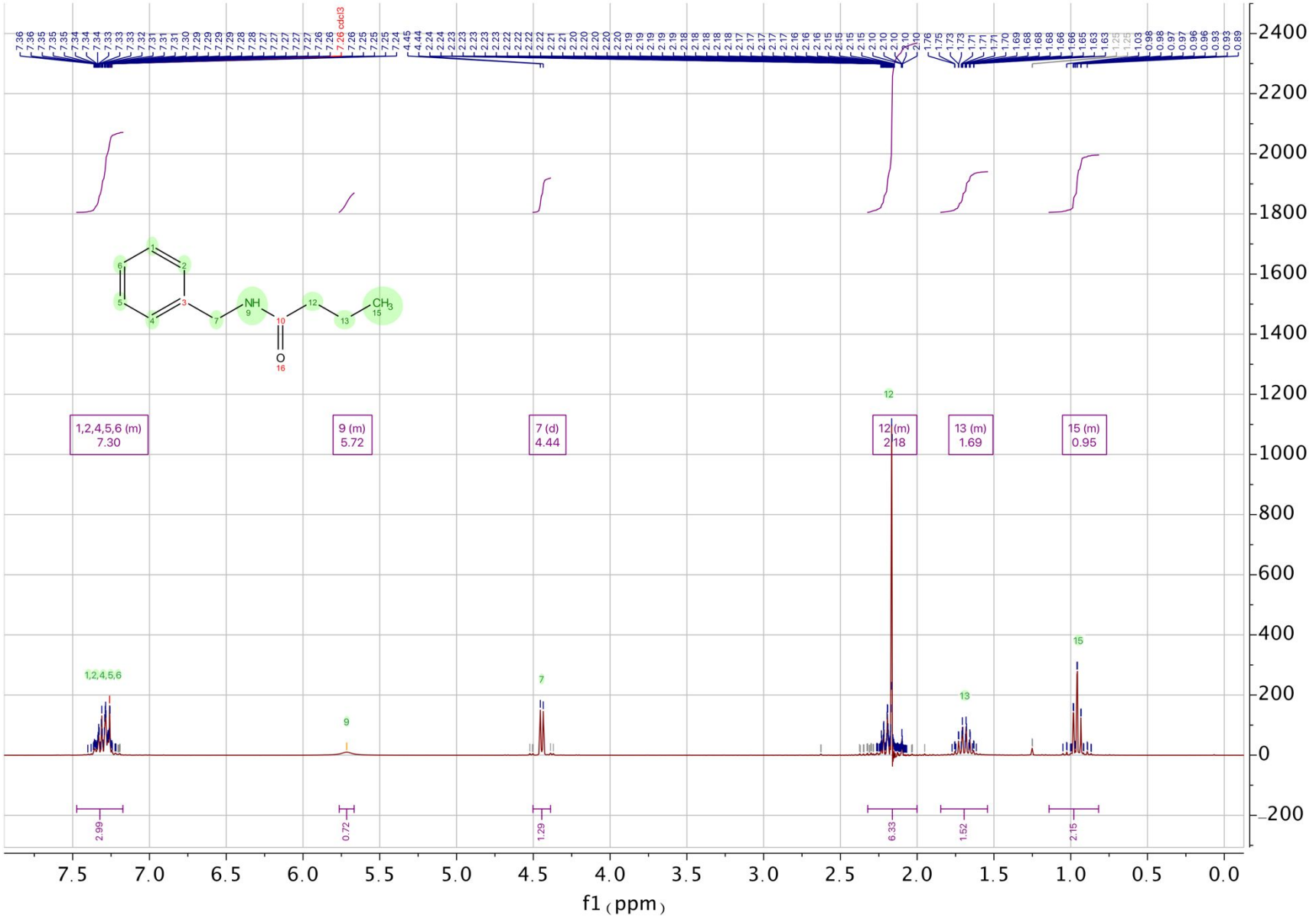

Figure S1. [1]H NMR spectra of **1**.

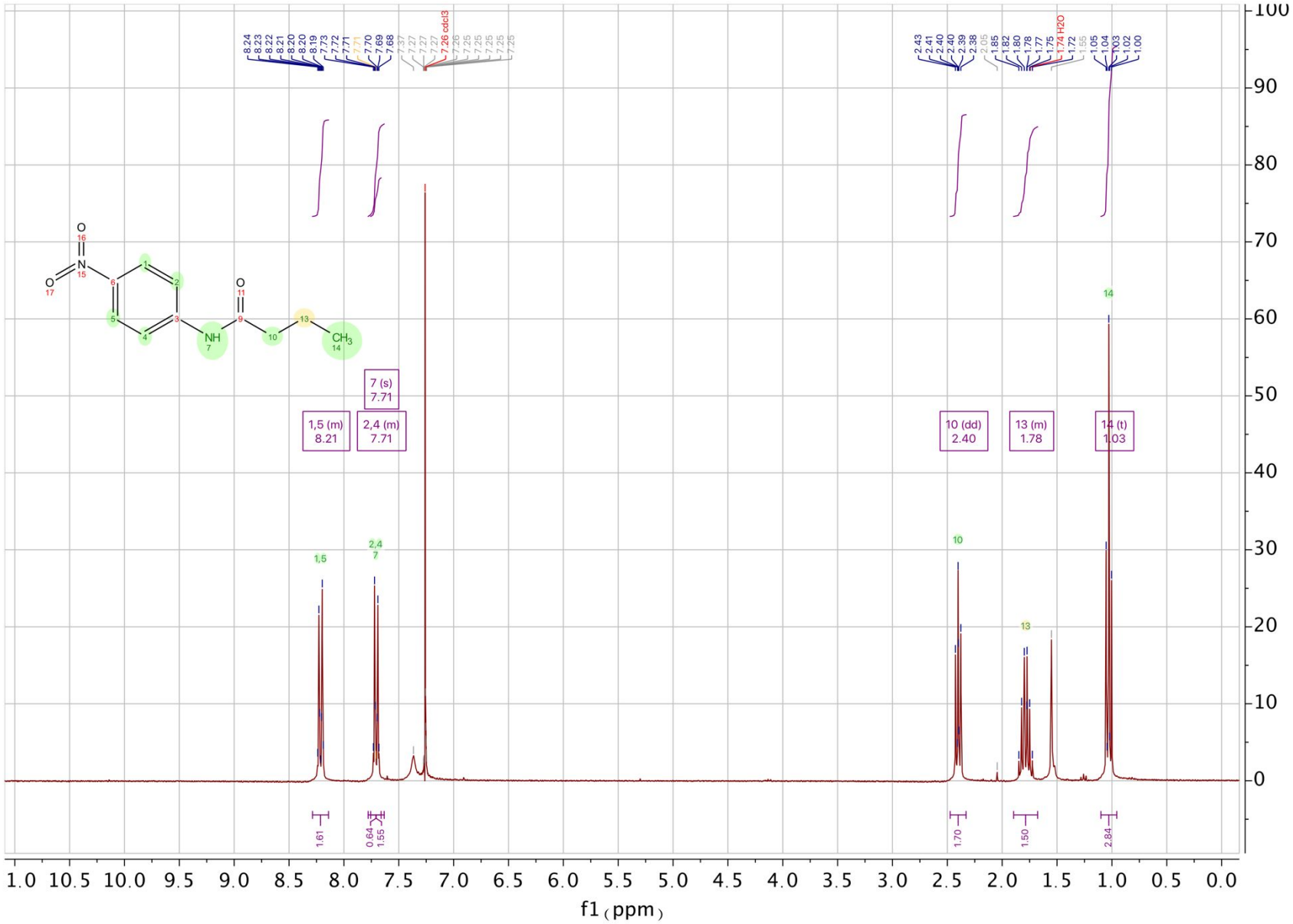

Figure S2. ^{1}H NMR spectra of **2**.

Classic MD simulations

MD simulations were done in order to equilibrate the system containing **1** and **2** as substrates. The time dependent evolution of the RMSD for both systems is depicted in Figures S3 and S4.

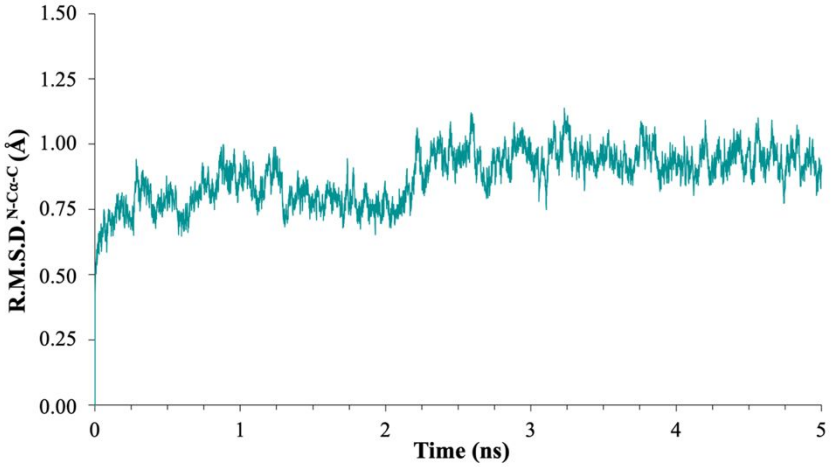

Figure S3. Time-dependent evolution of the RMSD of the atoms belonging to the protein backbone during the 5 ns MD trajectory of the **1**-CALB system.

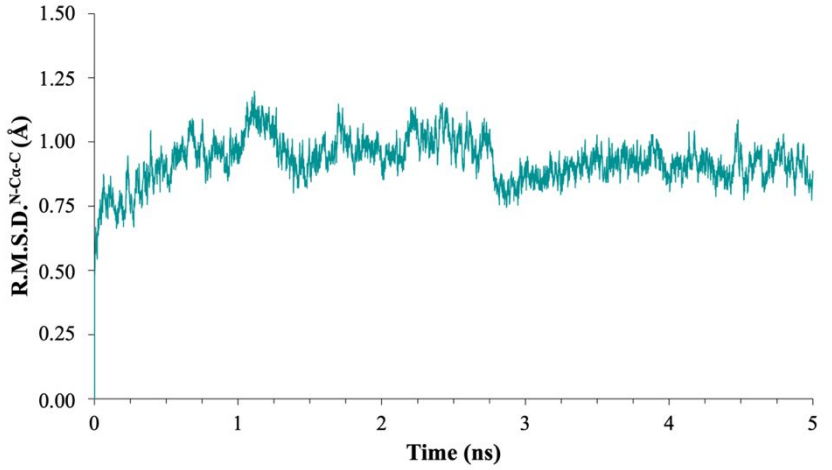

Figure S4. Time-dependent evolution of the RMSD of the atoms belonging to the protein backbone during the 5 ns MD trajectory of the **2**-CALB system.

QM/MM localized structures

Transition state structures localized at M06-2X level of theory are depicted in Figure S5. Averaged key distances of the structures localized at AM1/MM and M06-2X/MM are showed in Table S3 and Table S4 respectively. Averaged charges of key atoms were calculated from a QM/MM MD simulation at M06-2X/MM level and are shown in Table S5. Charges and polarization of the atoms belonging to the amide group of **2** produced by the residues belonging to the active site can be found in table S6.

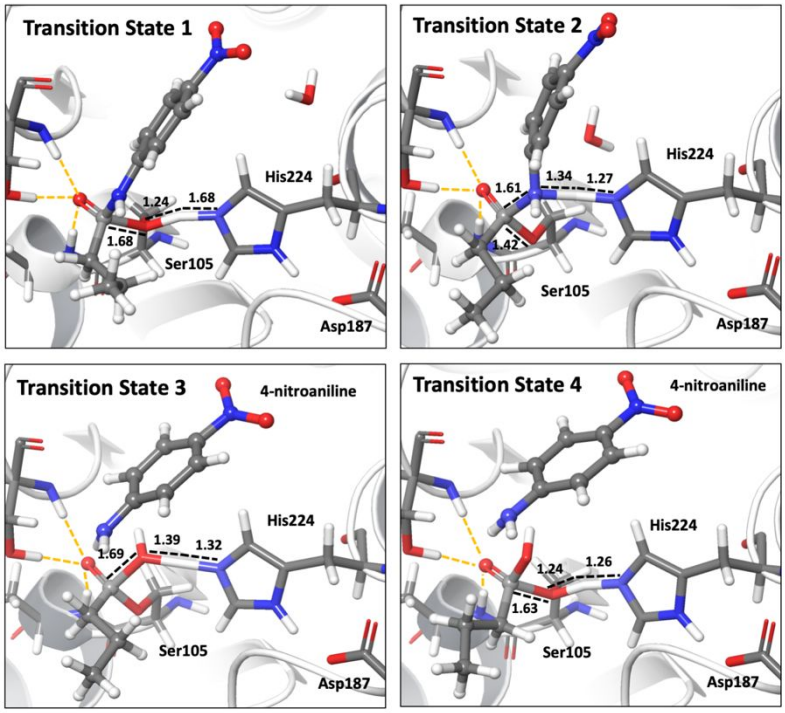

Figure S5 M06-2X/MM TS structures appearing along the hydrolysis of **2** catalyzed by CALB. Key protein residues are showed in liquorice, and substrate and products are showed in ball and sticks representation. Distances are in Å.

Table S3 Averaged key distances obtained from the structures located at AM1/MM level for the hydrolysis of **2** and used to compute averaged KIEs listed in Table S7.

	RS	TS1	TS2	TS3	TS4
OG_{Ser105}–$C1_{subs}$	2.51 ± 0.06	1.605 ± 0.012	1.4424 ± 0.0019	1.4199 ± 0.0014	1.538 ± 0.006
OG_{Ser105} – HG_{Ser105}	0.9631 ± 0.0005	1.299 ± 0.016	2.28 ± 0.05		
$NE2_{His224}$–HG_{Ser105}	2.37 ± 0.07	1.245 ± 0015	1.253 ± 0.006	-	-
$C1_{subs}$–$N4_{subs}$	1.3823 ± 0.0023	1.460 ± 0.005	1.556 ± 0.005	-	-
HG_{Ser105}–$N4_{subs}$	2.78 ± 0.05	2.68 ± 0.03	1.393 ± 0.013	-	-
O_{wat}–$C1_{subs}$	-	-	-	1.51 ± 0.24	1.4 ± 0.3
O_{wat}–$H1_{wat}$	-	-	-	1.273 ± 0.011	2.26 ± 0.03
$H1_{wat}$–$NE2_{His224}$	-	-	-	1.256 ± 0.012	1.252 ± 0.009
$H1_{wat}$ – OG_{Ser105}				2.289 ± 0.024	1.292 ± 0.007
$C1_{Ser105}$–$O2_{subs}$	1.2589 ± 0.0020	1.2928 ± 0.0011	1.3053 ± 0.0011	1.2980 ± 0.0014	1.2928 ± 0.0009
$O2_{subs}$–H_{Thr40}	1.94 ± 0.08	1.79 ± 0.05	1.78 ± 0.06	1.72 ± 0.03	1.82 ± 0.04
$O2_{subs}$–HO_{Thr40}	1.92 ± 0.04	1.90 ± 0.03	1.86 ± 0.04	1.843 ± 0.018	1.82 ± 0.04
$O2_{subs}$–H_{Gln106}	2.17 ± 0.18	1.90 ± 0.04	2.03 ± 0.07	1.91 ± 0.03	1.94 ± 0.04

Table S4 Key inter-atomic distances of the different states appearing along the hydrolysis of **2** catalyzed by CALB. Structures optimized at M06-2X/MM level. All distances are given in Å.

	RS	TS1	INT1	TS2	INT2	TS3	INT3	TS4	PS
$OG_{Ser105} - C1_{subs}$	2.32	1.68	1.51	1.42	1.32	1.39	1.43	1.63	2.20
$OG_{Ser105} - HG_{Ser105}$	1.00	1.24	1.81	2.50	2.53	-	-	-	-
$NE2_{His224} - HG_{Ser105}$	1.65	1.26	1.04	1.27	2.91	-	-	-	-
$C1_{subs} - N4_{subs}$	1.36	1.44	1.48	1.61	2.84	-	-	-	-
$HG_{Ser105} - N4_{subs}$	2.76	2.66	2.74	1.34	1.02	-	-	-	-
$O_{wat} - C1_{subs}$	-	-	-	-	4.33	1.69	1.49	1.40	1.33
$O_{wat} - H1_{wat}$	-	-	-	-	0.97	1.17	1.60	2.40	2.55
$H1_{wat} - NE2_{His224}$	-	-	-	-	3.77	1.32	1.05	1.26	1.64
$H1_{wat} - OG_{Ser105}$	-	-	-	-	4.78	2.61	2.78	1.24	1.00
$HD1_{His224} - OD2_{Asp187}$	2.02	2.08	2.04	2.19	2.15	2.18	2.14	2.03	2.00
$C1_{subs} - O2_{subs}$	1.26	1.29	1.31	1.30	1.23	1.30	1.32	1.29	1.24
$O2_{subs} - H_{Thr40}$	1.77	1.77	1.68	1.82	1.86	1.95	1.88	1.97	1.85
$O2_{subs} - HO_{Thr40}$	1.85	1.87	1.65	1.81	1.66	1.97	1.77	1.88	1.66
$O2_{subs} - H_{Gln106}$	2.14	1.95	1.78	2.05	1.85	1.93	1.79	1.89	1.91

Table S5. Charges of the key atoms of the **2** computed with the CHelpG method at M06-2X/MM level as an average of 20 ps MD simulations on the states involved in the full chemical reaction, from reactants state (RS) to Products state (PS). N4 only participates in the first two steps of the reaction. Charges are in a.u.

	C1	O2	N4
RS	0.85 ± 0.03	-0.884 ± 0.012	-0.77 ± 0.03
TS1	0.92 ± 0.04	-1.009 ± 0.020	-0.888 ± 0.023
INT1	1.04 ± 0.03	-1.104 ± 0.017	-0.89 ± 0.03
TS2	0.85 ± 0.04	-1.086 ± 0.015	-0.49 ± 0.03
INT2	0.82 ± 0.03	-0.806 ± 0.013	-0.78 ± 0.04
TS3	0.74 ± 0.04	-0.965 ± 0.022	-
INT3	0.73 ± 0.03	-1.039 ± 0.015	-
TS4	0.96 ± 0.04	-1.030 ± 0.021	-
PS	0.76 ± 0.03	-0.848 ± 0.013	-

Table S6. Charges of the key atoms of **2** computed with the CHelpG method at M06-2X/MM level in gas phase and including, as point charges, the atoms of the residues belonging to the oxyanion hole formed by residues Thr40 and Gln106 (Oxyanion), the residues Ser105, His224, and Asp187 (Catalytic Triad), residues Thr40, Gln106, Ser105, His224, and Asp187 (Oxyanion hole + Catalytic Triad), and the full protein. Charges are in a.u.

Atom	Gas Phase	Oxyanion Hole	Catalytic Triad	Oxyanion Hole + Catalytic Triad	Full Protein
C1	0.78	0.87	0.98	1.10	1.11
O2	-0.56	-0.79	-0.71	-0.91	-0.94
N4	-0.77	-0.72	-0.95	-0.98	-0.97

Determined Kinetic Isotope Effects

Averaged KIE at AM1/MM level are showed in table S7. As explained above, 10 structures of RS and each TS were localized at AM1/MM and averaged KIE were computed. Slightly differences on key distances and KIE exist between M06-2X/MM and AM1/MM which may be due to differences in the computed charges of the methods.

Table S7 Averaged KIEs computed at AM1/MM level for the reaction of hydrolysis of **2**.

	TS1	TS2	TS3	TS4
^{14}[1-C]	1.043 ± 0.005	1.016 ± 0.005	0.999 ± 0.004	1.007 ± 0.004
^{15}[4-N]	1.0008 ± 0.0021	1.0006 ± 0.0021	-	-
^{18}[2-O]	0.994 ± 0.004	0.992 ± 0.004	0.981 ± 0.005	0.987 ± 0.003

It is interesting to stress that the KIEs values obtained at M06-2X/MM level (see Table 1 of the text) are in good agreement to those average values calculated at AM1/MM level (see Table S6) in the case of ^{14}C and ^{15}N substitutions. On the contrary, the ^{18}O-KIE values at AM1/MM level (see Table S6) are slightly inverse, from 0.6 to 1.9 %. This can be rationalized based on the analysis of the inter-atomic interactions established between O2 and the residues of the oxyanion hole (Thr40 and Gln106). In all TS structures localized at AM1/MM, O2 atom forms stronger H-bond interaction than in the reactants state, due to the accumulation of negative charge of this atom along the reaction. This result explains the inverse ^{18}O-KIEs obtained at AM1/MM level. This effect is not so dramatic at M06-2X/MM level, where the variations of the distances between O2 atom and the residues of the oxyanion hole from reactants state to the different TSs, are not so meaningful (see Table S4).

Kinetics of hydrolysis of 2

Hydrolysis of **2** by CALB was evaluated at increasing concentrations of substrate as explained above. A Michaelis-Menten curve was fitted on the data (Figure S6), and kinetics constants were measured.

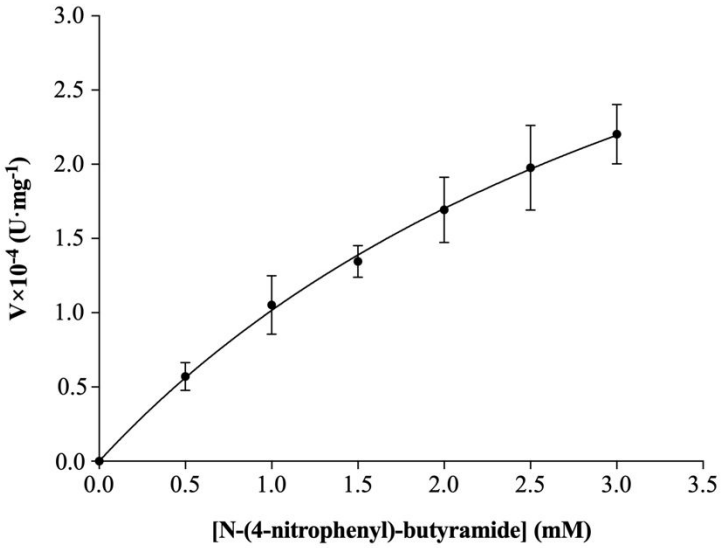

Figure S6. Kinetics of the hydrolysis of 2 by CALB. Velocities were calculated at increasing concentrations of substrate.

REFERENCES

(1) Uppenberg, J.; Morgens, H.; Shamkant, P.; Alwyn, J. T. The Sequence, Crystal Structure Determination and Refinement of Two Crystal Forms of Lipase B from Candida Antarctica. *Structure* **1994**, *2*, 293–308.

(2) Olsson, M. H. M.; SØndergaard, C. R.; Rostkowski, M.; Jensen, J. H. PROPKA3: Consistent Treatment of Internal and Surface Residues in Empirical p Kapredictions. *J. Chem. Theory Comput.* **2011**, *7*, 525–537.

(3) Søndergaard, C. R.; Olsson, M. H. M.; Rostkowski, M.; Jensen, J. H. Improved Treatment of Ligands and Coupling Effects in Empirical Calculation and Rationalization of PKa Values. *J Chem Theory Comput* **2011**, *7*, 2284–2295.

(4) Świderek, K.; Martí, S.; Moliner, V. Theoretical Study of Primary Reaction of Pseudozyma Antarctica Lipase B as the Starting Point to Understand Its Promiscuity. *ACS Catal.* **2014**, *4*, 426–434.

(5) Wang, J.; Wang, W.; Kollman, P. A.; Case, D. A. Automatic Atom Type and Bond Type Perception in Molecular Mechanical Calculations. *J. Mol. Graph. Model.* **2006**, *25*, 247–260.

(6) Zhang, W. E. I.; Yang, R.; Cieplak, P.; Luo, R. A. Y.; Lee, T.; Caldwell, J.; Wang, J.; Kollman, P. A Point-Charge Force Field for Molecular Mechanics Simulations of Proteins Based on Condensed-Phase. *J. Comput. Chem.* **2003**, *24*, 1999–2012.

(7) Phillips, J. C.; Braun, R.; Wang, W. E. I.; Gumbart, J.; Tajkhorshid, E.; Villa, E.; Chipot, C.; Skeel, R. D.; Poincare, H. Scalable Molecular Dynamics with NAMD. *J. Comput. Chem.* **2005**, *26*, 1781–1802.

(8) Dewar, M. J. S.; Zoebisch, E. G.; Healy, E. F.; Stewart, J. J. P. Development and Use of Quantum Mechanical Molecular Models. 76. AM1: A New General Purpose Quantum Mechanical Molecular Model. *J. Am. Chem. Soc.* **1985**, *107*, 3902–3909.

(9) Baker, J. An Algorithm for the Location of Transition States. *J. Comput. Chem.* **1986**, *7*,

385–395.

(10) Fukui, K. The Path of Chemical Reactions - The IRC Approach. *Acc. Chem. Res.* **1981**, *14*, 363–368.

(11) Zhao, Y.; Truhlar, D. G. The M06 Suite of Density Functionals for Main Group Thermochemistry, Thermochemical Kinetics, Noncovalent Interactions, Excited States, and Transition Elements: Two New Functionals and Systematic Testing of Four M06-Class Functionals and 12 Other Function. *Theor. Chem. Acc.* **2008**, *120*, 215–241.

(12) Frisch, M. J.; Trucks, G. W.; Schlegel, H. B.; Scuseria, G. E.; Robb, M. A.; Cheeseman, J. R.; Scalmani, G.; Barone, V.; Mennucci, B.; Petersson, G. A.; Nakatsuji, H.; Caricato, M.; Li, X.; Hratchian, H. P.; Izmaylov, A. F.; Bloino, J.; Zheng, G.; Sonnenberg, J. L.; Hada, M.; Ehara, M.; Toyota, K.; Fukuda, R.; Hasegawa, J.; Ishida, M.; Nakajima, T.; Honda, Y.; Kitao, O.; Nakai, H.; Vreven, T.; Montgomery, J. A., Jr.; Peralta, J. E.; Ogliaro, F.; Bearpark, M.; Heyd, J. J.; Brothers, E.; Kudin, K. N.; Staroverov, V. N.; Kobayashi, R.; Normand, J.; Raghavachari, K.; Rendell, A.; Burant, J. C.; Iyengar, S. S.; Tomasi, J.; Cossi, M.; Rega, N.; Millam, J. M.; Klene, M.; Knox, J. E.; Cross, J. B.; Bakken, V.; Adamo, C.; Jaramillo, J.; Gomperts, R.; Stratmann, R. E.; Yazyev, O.; Austin, A. J.; Cammi, R.; Pomelli, C.; Ochterski, J. W.; Martin, R. L.; Morokuma, K.; Zakrzewski, V. G.; Voth, G. A.; Salvador, P.; Dannenberg, J. J.; Dapprich, S.; Daniels, A. D.; Farkas, O.; Foresman, J. B.; Ortiz, J. V.; Cioslowski, J.; Fox, D. J. Gaussian 09, Revision E.01. Gaussian, Inc.: Wallingford, CT 2009.

(13) Roux, B. The Calculation of the Potential of Mean Force Using Computer-Simulation. *Comput. Phys. Commun.* **1995**, *91*, 275–282.

(14) Torrie, G. M.; Valleau, J. P. Non-Physical Sampling Distibutions in Monte-Carlo Free-Energy Estimation - Umbrella Sampling. *J. Comput. Phys.* **1977**, *23*, 187–199.

(15) Kumar, S.; Rosenberg, J. M.; Bouzida, D.; Swendsen, R. H.; Kollman, P. A. The Weighted Histogram Analysis Method for Free-energy Calculations on Biomolecules. I. The Method. *J. Comput. Chem.* **1992**, *13*, 1011–1021.

(16) Verlet, L. Computer “Experiments” on Classical Fluids. I. Thermodynamical Properties of

Lennard-Jones Molecules. *Phys. Rev.* **1967**, *159*, 98–103.

(17) Martí, S.; Moliner, V.; Tuñón, I.; Williams, I. H. QM / MM Calculations of Kinetic Isotope Effects in the Chorismate Mutase Active Site. *Org. Biomol. Chem.* **2003**, *1*, 483–487.

(18) Martí, S.; Moliner, V.; Tuñón, I. Improving the QM/MM Description of Chemical Processes: A Dual Level Strategy to Explore the Potential Energy Surface in Very Large Systems. *J. Chem. Theory Comput.* **2005**, *1*, 1008–1016.